Available online at www.sciencedirect.com

ScienceDirect

journal homepage: www.elsevier.com/locate/he

An experimental analysis of PEMFC stack assembly using strain gage sensors

Christophe Carral [a], Nicolas Charvin [a], Hélène Trouvé [b], Patrice Mélé [a,*]

[a] LEPMI, UMR 5279, CNRS, Grenoble INP – Université de Savoie – Université J. Fourier, LMOPS – INES, Bât. IUT, Campus Savoie Technolac, F-73376 Le Bourget-du-Lac Cedex, France
[b] Axane, 2 rue de Clémencière, 38360 Sassenage, France

ARTICLE INFO

Article history:
Received 6 November 2013
Received in revised form
3 January 2014
Accepted 8 January 2014
Available online 12 February 2014

Keywords:
Proton Exchange Membrane Fuel Cell
Stack assembly
Strain gage
Mechanical properties

ABSTRACT

This work investigates the mechanical state of Proton Exchange Membrane Fuel Cells (PEMFC) during its assembly, essential for the system efficiency. By the mean of strain gage sensors and optical measurements, the influence of the number of cells and the clamping method are investigated on stacks composed of 1–16 cells. Two different solicitations are applied: ideal and real assembly conditions. The ideal conditions reveal the effect of the number of cells on the stack properties whereas the end-plates deflection and deformations can inform us about the compression ratio distribution of the active layer of the cell (MEA) under real assembly conditions. The method proposed here can be incorporated in existing systems, and provide relevant informations to optimize the stack performance.

1. Introduction

The assembly process of polymer electrolyte membrane fuel cells (PEMFC) is a critical step to set up the system performance [1–9]. The stack is a sandwich-like structure composed of many layers, materials and interfaces (Fig. 1). First the MEA, composed of the gas diffusion layer (GDL), the catalyst layer (CL) and the membrane, is embedded between two bipolar plates (BPP), forming the reference cell. Gaskets are afterward added to prevent gas leakages. This cell is then multiplied as needed, according to the power and voltage required. All these layers are generally assembled between two rigid end-plates (EP). Three types of clamping design are usually used: (i) point-load design, (ii) line-load design and (iii) surface-load design; the point-load design being the most common one [10].

Several studies have been proposed in the literature to reach the optimal performance of PEMFC stacks according to the clamping force [1–9]. Most of these studies were however focused on stacks composed of a single-cell, clamped with different tie-rod configurations. For each stack studied, the PEMFC performance varied with the magnitude of the clamping force. Two opposite effects were then identified with the clamping force increase [7–9,11]:

- the contact pressure between the bipolar plate and the MEA (*Pc*) rises, leading to a reduction of the electrical contact resistance,
- the MEA compression ratio (*CR*) increases, crushing the GDL pores and thus increasing the gas transport resistance within the GDL.

* *Corresponding author*. Tel.: +33 479 75 9434; fax: +33 479 75 8840.
E-mail addresses: christophe.carral@univ-savoie.fr (C. Carral), patrice.mele@univ-savoie.fr, pmele@univ-savoie.fr (P. Mélé).
0360-3199/$ – see front matter
http://dx.doi.org/10.1016/j.ijhydene.2014.01.033

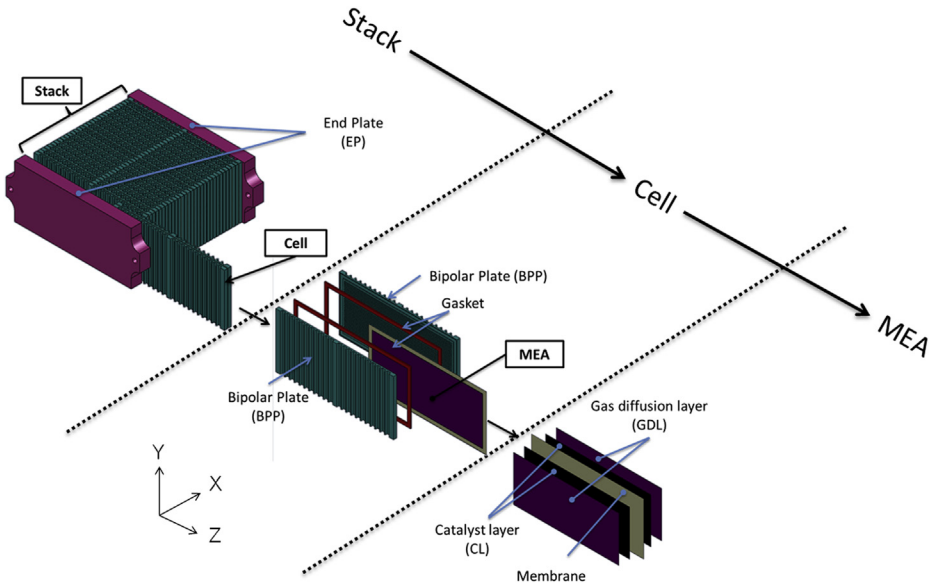

Fig. 1 – Description of the different stack components.

As it can be inferred from the above, an optimal clamping force, depending on the stack design, can be identified by establishing a balance between the reduction of the electrical resistance and the limitation of the gas transport.

These two phenomena are directly related to the mechanical state of the MEA; its stress and strain amplitude governing respectively the *Pc* and the *CR* values. An optimal value of the *Pc*, or the *CR*, has to be reached in order to get the best performance of the stack. Nitta et al. [11] and Hottinen et al. [12] have shown that the non-uniformity of the GDL compression has an adverse effect on the current density distribution and tends to alter the lifetime and the local performance of the cell. These studies confirmed the necessity to apply a uniform deformation on the active layers of the cell during assembly.

The evaluations of the parameters *Pc* and *CR* are generally performed at a global scale. The difference of stack lengths, before and after its clamping, divided by the number of the cells, allows in fact the determination of the global *CR* value. Ge et al. [3] or Chang et al. [4] developed special fixtures to measure the *CR* value on a single-cell. By the mean of rigid EPs and dial gages, these apparatus compress MEAs in a more uniform way. Lin et al. [8] and Escribano et al. [9] used several gaskets with different thicknesses to control the MEA compression on a single-cell. In all these studies, measurements of PEMFC performance were performed and have confirmed that an optimal MEA compression ratio exists. Others authors proposed to evaluate the *Pc* value and its distribution by using (i) pressure sensitive films [1,2,13,14] or (ii) piezoresistive film sensors [6,7,15,16]. With the exception of Wen et al. [2], all these studies were based on PEMFC stacks composed of a single-cell. These two techniques have been able to define the optimal conditions of clamping, by observing the imprint of the films, after the disassembly of the stack. They remain however limited to comparative measurements, as they are dependent on the design, manufacturing tolerances and form errors of BPPs [10].

As a complement of these techniques, a novel experimental method is proposed in this article. The uniformity of the MEAs mechanical state in the stack is investigated through the evaluation of the EP deflection and strains, using strain gages. The tie-rods used for the clamping have also been instrumented to measure the force applied on the stack during its assembly. To contribute to the existing studies mainly made on single-cells, the developed equipment is used to analyze the effect of the number of cells on the stack mechanical state. Two cases are considered in order to separate the influence of the clamping force and the number of cells on the mechanical response of the stack. The first one is characteristic of an “ideal” assembly of stacks composed of a variable number of cells, ranging from 1 to 16; the second one mimics the real case, i.e. an assembly by one pair of tie-rods.

2. Materials and methods

The experimentations were carried out on stacks based on PEMFC systems manufactured by Axane company. The latter were composed of rectangular carbon composite BPPs with parallel serpentine flow fields with an active area of 85 cm^2. The same 16 pairs of BPPs were used for every tests. MEAs were renewed for each test to avoid the influence of plastic deformations which could occur during previous compression tests. The GDL composing the MEA were carbon paper type. The gaskets were not included during these tests as they were silicon based with low Young modulus, which tend to limit their influence on the global mechanical stiffness. Preliminary measurements showed, in point of fact, that the force supported by the gasket represents only 5% of the global clamping load [17]. This component will be then considered as negligible from a mechanical point of view.

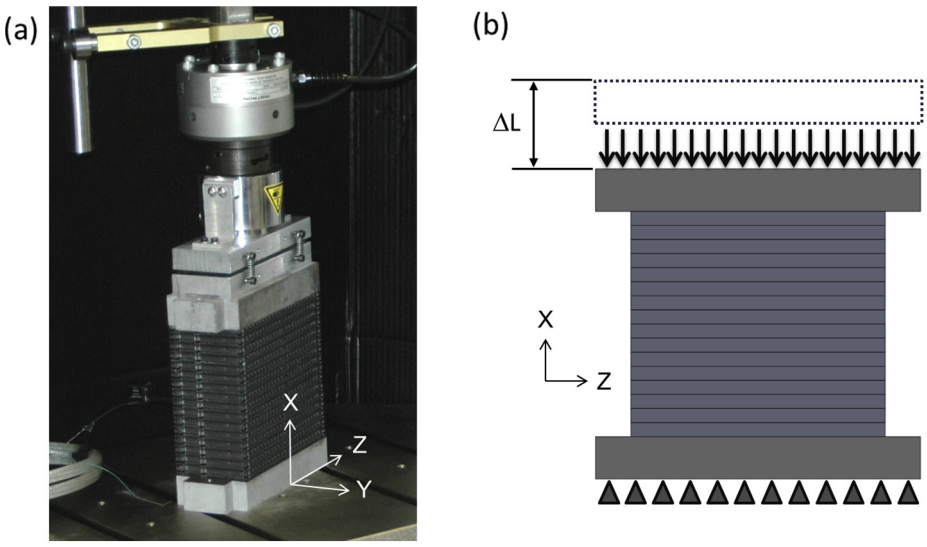

Fig. 2 – (a) Picture of the fixture for ideal assembly condition tests and (b) its schematic representation.

2.1. *Ideal assembly conditions*

An Instron 8872 test bench with specific devices (Fig. 2) was used to simulate ideal assembly conditions on stacks composed of 1–16 cells. Since the tests required a large amount of MEA, only one test per stack was performed, except for the tests on single-cell where 3 experiments were replicated. End-plates in steel with a thickness of 30 mm were used in the different experiments to limit the bending, and thus obtain a quasi-uniform compression state. A deflection inferior to 5 μm, considered as negligible in the next parts of this study, was evaluated on the upper EP by the method of digital image correlation. The lower end-plate was mechanically anchored on the frame of the machine, prohibiting its bending. The force was applied on the upper EP through a specific system, using a ball trapped between two plates in order to allow rotation of the upper plate. The goal of this system was to adapt itself to the geometry of the stack and to reduce the effects caused by the addition of manufacturing errors.

The displacement of the upper EP (ΔL) was measured on both sides (front and rear) of the stack, in order to verify the possible rotation of the upper plate. On the front, digital images correlation was used to measure the displacement of the EP at a macro scale, and the relative displacement between two BPPs of each cell at a meso scale. Pictures were taken with a Nikon D5100 equipped with a macro lens (ref. Nikon micro Nikkor 105 mm) and a ring flash (ref. Sigma EM-140 DG). The displacements were evaluated from the pictures with the 7D software [18]. The measurements on the rear of the stack were performed by a standard extensometer (ref. Instron 2620-601).

14 steps of loading were applied, with a clamping force F within the range of 100–10 000 N. A minimum value of 100 N was taken into account to put all elements in contact. Based on the average of the displacement measurements, evaluated

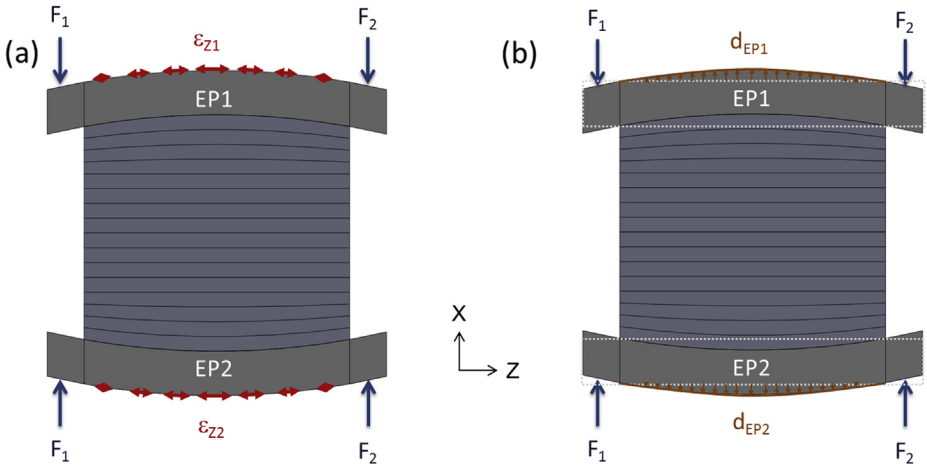

Fig. 3 – Representation of (a) the deformations ε_Z and (b) the deflection d_{EP} of the stack EPs, due to the bending under real assembly conditions.

on both sides of the stack, the CR parameter was calculated via the following equation:

$$CR = \frac{\Delta L_{Front} + \Delta L_{Rear}}{2 \cdot N_{Cells} \cdot th_{MEA}} \quad (1)$$

with ΔL_{Front} and ΔL_{Rear} the upper EP displacements measured on the front and rear of the stack respectively, N_{Cells} the number of cells, and th_{MEA} the average initial thickness of the MEAs.

The deformations of the BPPs were considered as negligible in this part. Only MEAs were considered as compressible. This calculation supposes moreover that the CR was equally divided between all MEAs of the stacks. Such an assumption had been firstly validated by the digital images correlation measurements.

2.2. *Real assembly conditions*

The same stack was used to study the deformations during real assembly conditions. In this setting, the stack was clamped between two 15 mm thick aluminum EPs by a traditional point-load design, composed of one pair of tie-rods. A bending could thus occur on the different parts, in particular on the EPs (Fig. 3). A specific bench was then developed to measure simultaneously i) the global clamping force ($F = F_1 + F_2$), ii) the EP strain due to the bending ($\varepsilon_{Z1\ \&\ 2}$) and iii) the EP deflection ($d_{EP1\ \&\ 2}$).

To evaluate the evolution of the force during the clamping, 4 strain gages were bonded on the 2 tie-rods (Fig. 4). Two gages measured the longitudinal strain due to the tie-rods elongation under application of the clamping force (G1 and G3), and two others measured the transversal strain (G2 and G4). This configuration is typical for load cell transducers [19]. Each instrumented tie-rod, called I-TieRod1 & 2, was firstly calibrated as force sensors with an Instron 8872 test bench equipped with a 5 kN load cell.

Several strain gages were placed on the two EPs, called I-EP1 & 2, to evaluate the strain, ε_Z, at different locations. Seven strain gages were placed on the I-EP1 (Fig. 5) and one strain gage was bonded at the center of the I-EP2. The strain gages used were typical metallic foil gages. A Vishay System 7000 was used for signal treatment and data acquisition.

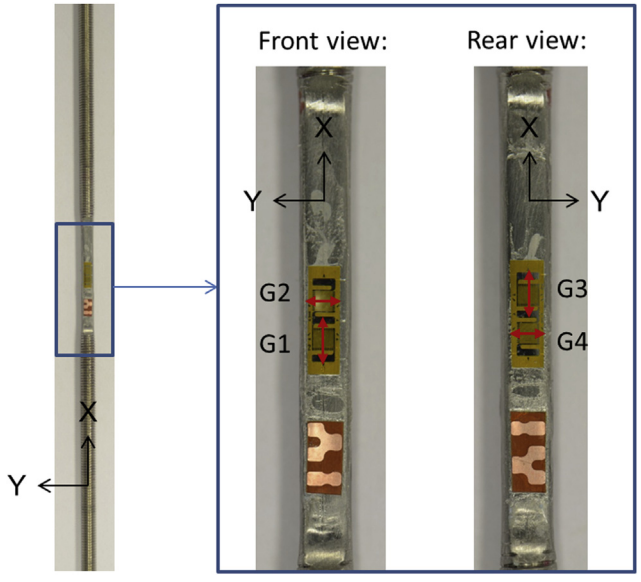

Fig. 4 – Force sensor (I-TieRod).

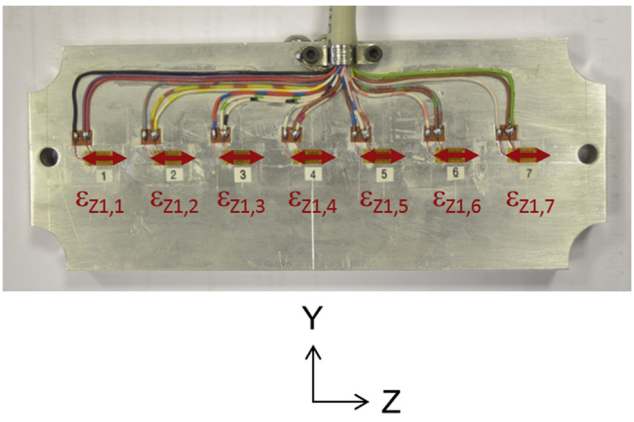

Fig. 5 – Strains sensor (I-EP).

The stack equipped with these 4 specific sensors (I-TieRod1 & 2, I-EP1 & 2) was then placed on the table of a Microvu Vertex 410 optical measuring center to measure the EPs deflection d_{EP} (Fig. 6). This equipment allows measurements with ±1.6 μm minimum accuracy.

To evaluate the displacements, $d_{EP1\ \&\ 2}$, for each step of loading, a minimum of 2000 points were recorded on the external upper edges of both EPs (orange lines on Fig. 3b) by the optical measuring equipment. Note that the EP portions used to support the tie-rods were not taken in account into the deflection evaluation. First a clamping force of 100 N was applied on the stack, necessary for contacting every element. These first data were then considered as "baseline" and were deducted from the following measurements. A 4th degree polynomial was finally used to fit the measured points. The justification of such a polynomial fit will be discussed in Section 3.2.

Six steps of loading were applied with F in the range of 100–5000 N. The forces on each tie-rod, F_1 and F_2, were progressively increased by turning the nuts, while maintaining a

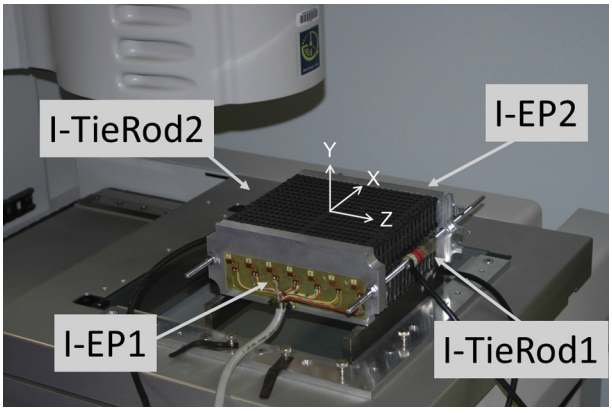

Fig. 6 – A 16 cell stack with force and strain sensors on the optical measuring center table.

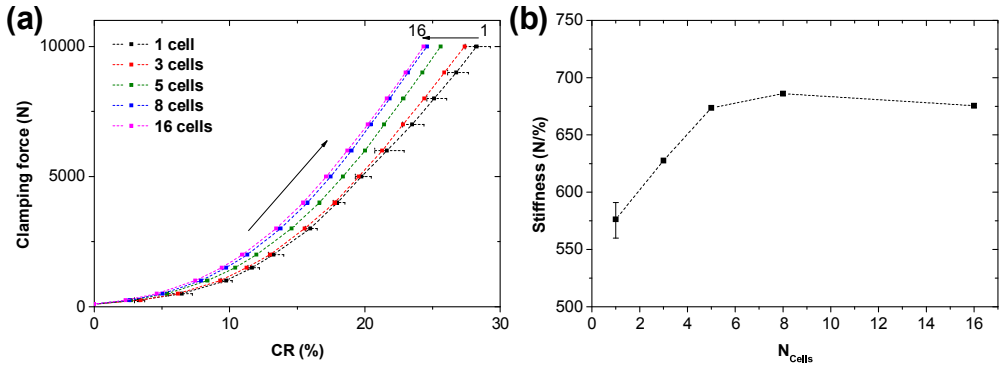

Fig. 7 – (a) Variations of the CR versus the clamping force at macro scale, on stacks composed of 1–16 cells, and (b) average stiffness of the stacks, for a clamping force within the range of 4000–10 000 N.

good equilibrium between the two loads. For each step, the force on the stack, the strains on both EPs and the deflection were recorded. Three distinct tests were performed, assuring that each test had been made with new MEAs. Two stacks, including 8 and 16 cells, were used.

3. Results and discussion

3.1. *Ideal assembly conditions*

Fig. 7(a) shows the evolution of the clamping force versus the CR for stacks composed of 1–16 cells. The curves show a nonlinear behavior with a significant hardening effect with increasing the clamping force. This specific behavior of GDL is consistent with previously published works [9,20,21]. For a clamping force value higher than 4000 N, a quasi-linear behavior can be observed. An equivalent stiffness can be then evaluated on this linear portion. A dependency on the number of cells is noticed: the increase in this variable, N_{Cells}, leads to a greater stack stiffness. This effect is particularly considerable for stacks composed of a small number of cells (1–5) before reaching a plateau (Fig. 7b). The determination of the elastic properties of the stack is not possible, given the impossibility of evaluating the exact contact area between the BPPs and the MEAs.

Increasing the number of cells leads to increase positioning and geometrical errors, due to the sum of all layers manufacturing tolerances. However, these errors tend to balance out when the number of cells increases. To confirm this interpretation, the difference of measurements on both sides of the stacks is depicted on Fig. 8. For a small number of cells, the CR values on the front side of the stack are always higher than that of on the rear, with a difference going up to 10%. By increasing the number of cells, this difference decreases; a similar result on both sides of the stack for 16 cells can be seen. We can also observe that the differences increase mostly for clamping force value ranging from 100 to 1000 N. If one considers the differences from a clamping force of 1000 N instead of 100 N, the curves tend to nearly coincide with a diminution of the difference to 2.5%, regardless of the number of cells (Fig. 8b). Accordingly, most of the differences happen for low levels of forces, implying that this phenomenon occurs when all layers get into contact. This demonstrates the major role played by the interfaces on the global behavior in this specific force field.

3.2. *Real assembly conditions*

Fig. 9 shows the experimental deflection (d_{EP1}) and strains (ε_{Z1}) of the I-EP1 for a stack composed of 16 cells. Both measurements show a symmetry on Z direction, with maximum

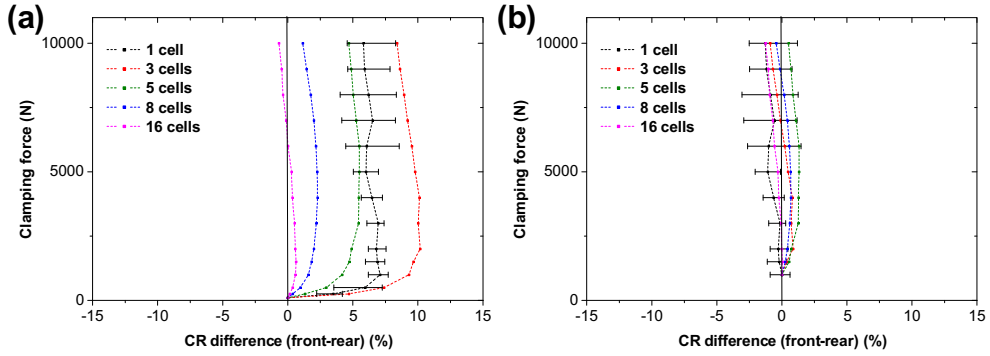

Fig. 8 – Evolution of the CR difference between the front and the rear of the stacks with 1-3-5-8-16 cells from a clamping force value of (a) 100 N and (b) 1000 N.

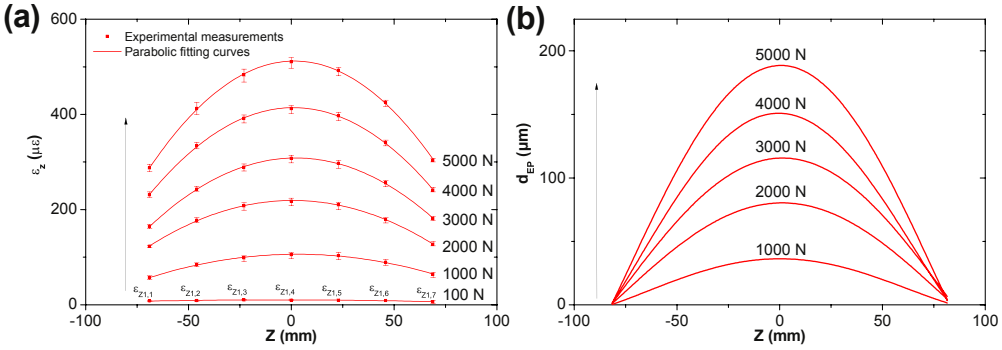

Fig. 9 – Experimental results on the I-EP1 of (a) the strains (ε_{Z1}) and (b) the deflection (d_{EP1}) for a 16 cell stack.

values located on the middle of the EP (Z = 0). ε_Z is positive, characteristic of a tensile state, in agreement with classical bending theory. Moreover, these strains follow a parabolic behavior, through the relation:

$$\varepsilon_Z = A + B \cdot Z + C \cdot Z^2 \quad (2)$$

where A, B and C are constants.

The values of the fitting parameters, presented in Table 1, have been obtained by minimizing the difference between experimental and predicted data, for the clamping forces used.

According to the Euler–Bernoulli theory [22], bending strains following a parabolic curve can be related to a beam subjected to a uniformly distributed load. A 4th degree polynomial can thus be used to predict the evolution of the deflection, consistent to our previous choice to smooth the data measured by the optical measuring equipment with a polynomial of this type (cf. Section 2.2).

On Figs. 10 and 11, the maximum values of $d_{EP1\ \&\ 2}$ and $\varepsilon_{Z1\ \&\ 2}$ are plotted versus the clamping force, for stacks composed of 8 and 16 cells respectively. Similar results are found, regardless of the number of cells used. Experiments show that the EPs response varies linearly with the clamping force in the range of 0–5000 N. Equivalent stiffnesses can be thus evaluated, with values close to 9.5 N/με for the strain stiffness and 27 N/μm for the deflection stiffness. The results on both EPs are moreover similar, showing an additional symmetry in X direction.

It is worth noting that this method could be used to calibrate the I-EPs as deflection and force sensors, in order to carry out in-situ measurements. Even without calibration, strain gages could be employed to evaluate continuously the EP strain, and thus shed light into the variations of the deflection and the compression force during the fuel cell operation, providing relevant information for the stack performance over time.

Table 1 – Parabolic fitting curves parameters.

F (N)	A (με)	B (με/mm)	C (με/mm^2)	R^2
100	1.0×10	-8.3×10^{-3}	-6.6×10^{-4}	0.922
1000	1.1×10^2	5.2×10^{-2}	-9.5×10^{-3}	0.997
2000	2.2×10^2	2.7×10^{-2}	-2.0×10^{-2}	0.999
3000	3.1×10^2	1.3×10^{-1}	-2.8×10^{-2}	0.999
4000	4.1×10^2	7.3×10^{-2}	-3.7×10^{-2}	0.999
5000	5.1×10^2	1.3×10^{-1}	-4.5×10^{-2}	0.999

3.3. Analytical model

3.3.1. Description

The Euler–Bernoulli beam theory can now be used to predict the stress, strains or displacements of the EPs in function of the clamping force. An analytical model has thus been developed (Fig. 12), based on the following assumptions:

- the EP is isolated and considered as a beam.
- On the outer side of the stack, two point forces F are applied, representing the contacts with the tie-rods.
- On the inner side of the stack, the definition of the boundary conditions is more complex. As a first approach, a uniformly distributed load is assumed (R_{DL}), in agreement with the experimental measurements (see Section 3.1).

A large discrepancy remains however between experimental and predicted data with this single reaction force (results not shown here). Consequently, a second point force has been added at the extremities of the BPPs, represented by the letter R on Fig. 12. The reaction forces on the inner side of the stack are then divided in two parts, R and R_{DL}. A parameter P, representing the relative contribution of these two forces, has been defined.

According to Euler–Bernoulli beam theory [22], the maximum strain on Z axis ε_Z and the deflection d resulting on X axis, are defined via the following expressions, as a function of the position on the beam Z:

$$\varepsilon_Z(Z) = \pm \frac{M(Z)}{EI} \times \frac{h}{2} \quad (3)$$

$$d(Z) = \iint \frac{M(Z)}{EI} d_Z^2 \quad (4)$$

with M the bending moment, E the Young modulus, I the moment of inertia and h the height of the beam. The sign of the strain depends of the position on the beam (top or bottom).

These definitions are used to develop the analytical model. Symmetry is integrated on Z axis, as shown by the

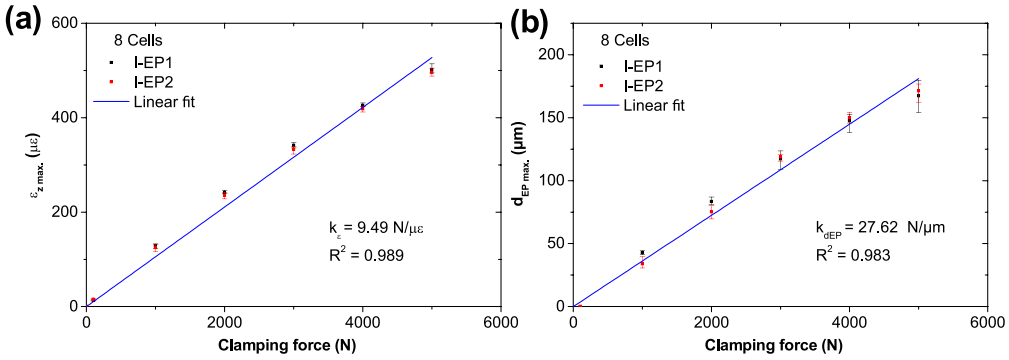

Fig. 10 – Experimental results of (a) $\varepsilon_{Zmax.}$ and (b) $d_{EPmax.}$ for a 8 cell stack.

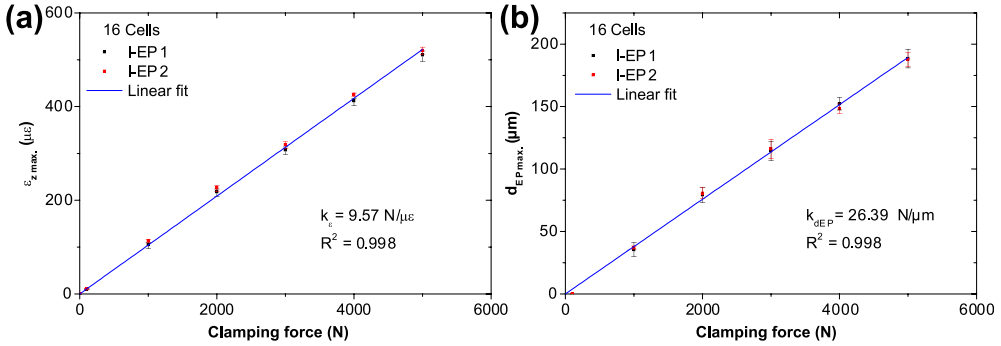

Fig. 11 – Experimental results of (a) $\varepsilon_{Zmax.}$ and (b) $d_{EPmax.}$ for a 16 cell stack.

experimental results, consequently only the left half of the system is studied. Based on the boundary conditions, two distinct regions (1 and 2) are considered. The equations describing this model are detailed in Table 2. All parameters are listed in Table 3.

3.3.2. *Comparison between experimental and predicted results*

Fig. 13 shows the comparison between experimental and predicted data, as a function of the clamping force. A good agreement is found for the EP strains ε_Z, measured by the strain gages, for $P = 0.45$. In this case, the EP deflection, d_{EP}, is slightly overestimated by the model, with differences going up to +8%. It is found that P must be equal to 0.55 in order to predict the experimental evolution of the EP deflection, previously determined through the optical measuring center (not shown here). The difference in values of P to fit the EP strains or its deflection could be explained by the greater sensibility of the deformations than that of the deflection. The simplifications made in the model on the geometry and the boundary conditions can be also responsible of these differences in P values. Note however that these values to fit the deformations or the deflection of the EP are close, and about equal to 0.5. This indicates that nearly half of the clamping force applied on the stack is supported by the borders of the BPP gas channels, whereas they represent less than 10% of the total contact area between the MEA and the BPP (Fig. 14). This provides a relevant information regarding the load distribution on the MEA, and on the CR distribution; an over

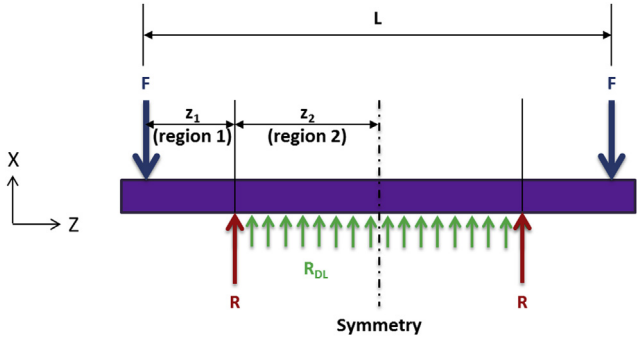

Fig. 12 – Analytical model.

Table 2 – Analytical model equations.

Region 1

$$\varepsilon_{Z,1}(Z') = \pm\frac{6\cdot F\cdot Z'}{E_{EP}\cdot b\cdot h^2}$$

$$d_{EP,1}(Z') = \frac{1}{E_{EP}\cdot I}\left(-\frac{F}{6}Z'^3 + C_{11}\cdot Z' + C_{12}\right)$$

Region 2

$$\varepsilon_{Z,2}(Z') = \pm\frac{3}{2}\frac{R_{DL}\cdot Z'^2 - 2(F+R_{DL}\cdot z_1 - R)\cdot Z' + R_{DL}\cdot z_1^2 - 2\cdot R\cdot z_1}{E_{EP}\cdot b\cdot h^2}$$

$$d_{EP,2}(Z') = \frac{1}{E_{EP}\cdot I}\left(\frac{R_{DL}}{24}Z'^4 - \frac{z_1\cdot R_{DL} - R + F}{6}Z'^3 + \frac{R_{DL}\cdot z_1^2 - 2\cdot R\cdot z_1}{4}Z'^2 + C_{21}\cdot Z' + C_{22}\right)$$

with

$Z' = Z - z_1 - z_2$

C_{11}, C_{12}, C_{21} and C_{22} the integration constants

Table 3 – Analytical model parameters.

Input parameters	Description	Unit
F	Applied point force (tie-rod force)	N
P	Proportion of the force F on R (between 0 and 1)	w/o
z_1	Distance between the application point of F and the BPP gas channel edging	mm
z_2	Distance between the BPP gas channel frame and the middle of the EP	mm
b	EP width (dimension in Y direction)	mm
h	EP height (dimension in X direction)	mm
E_{EP}	Young modulus of the EP material	MPa

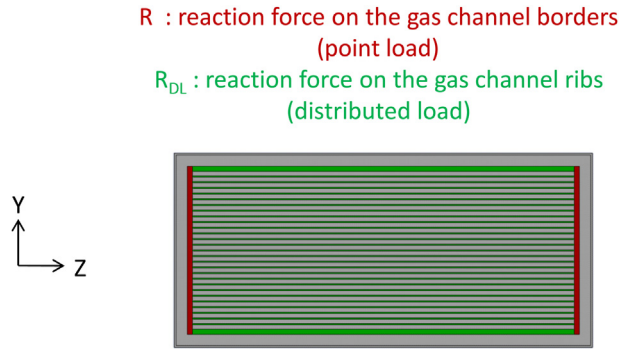

Fig. 14 – Schematic representation of the reaction forces on the BPPs gas channels.

compression of the MEA on the borders of the stack occurs, induced by the assembly method. This result is consistent with experimental published studies where an over compression has been observed as well on the border of cells [2,10,14–16].

Through the development of a new experimental method, this study shows that the stack assembly method is the cause of the distribution of the mechanical parameters around the optimal target. This could limit the PEMFC performance and potentially lead to a premature degradation of the MEAs.

4. Conclusions

The influence of the assembly conditions on the performance of PEMFC stacks is investigated, according to two different cases or situations. Ideal assembly conditions are, as a first step, imposed on stacks composed of 1–16 cells. It is shown that the increase of the number of cells tends to raise the stack stiffness. The sum of geometry errors, due in particular to the manufacturing process or positioning errors, leads to variations of the compressive behavior of the stack. These errors tend to balance out when the number of cells is greater than 5. According to these observations, the studies on stacks should be performed on a minimum number of cells, in order to limit the influence of cell positioning on the global behavior.

The second case studied is based on real conditions of stack assembly with a clamping device composed of a real point-load design. A specific bench has been developed, instrumented with strain sensors and placed on an optical measuring equipment. Such a device offers the potential to measure simultaneously the values of the deflection d_{EP} and the deformations ε_Z of both EPs, according to the clamping load amplitude. Similar results have been obtained on each end plate. A parabolic evolution of the EP strains has moreover been revealed. The maximum values of the deflection and the strain of the EP are directly related to the clamping force; a linear relation between these two parameters has indeed been demonstrated.

An analytical model has been then proposed in the second part of this study to predict the evolution of the EP deflection or strains with increasing the clamping load. This model distinguishes the relative contributions of the different sections of the BPP from the global mechanical behavior. A stress concentration effect has in particular been shown on the border of the BPP, with half of the clamping force supported by this part. Such a phenomenon generates an over-compression of the MEA at this location and has to be modified in future design of BPPs. To reduce this stress concentration effect, new assembly methods of stacks, exhibiting for example multiple tie rods or additional absorbing systems, have to be developed allowing greater performance of the stack.

To complete this experimental study mainly focused on a global scale, a 3D finite element model has been developed, allowing to determine at a lower scale the complete distribution of stresses and strains in the active layers and their respective influence on the electrical contact resistance and the GDL porosity change. These results will be published in a separate paper and will be compared to the experimental results shown here.

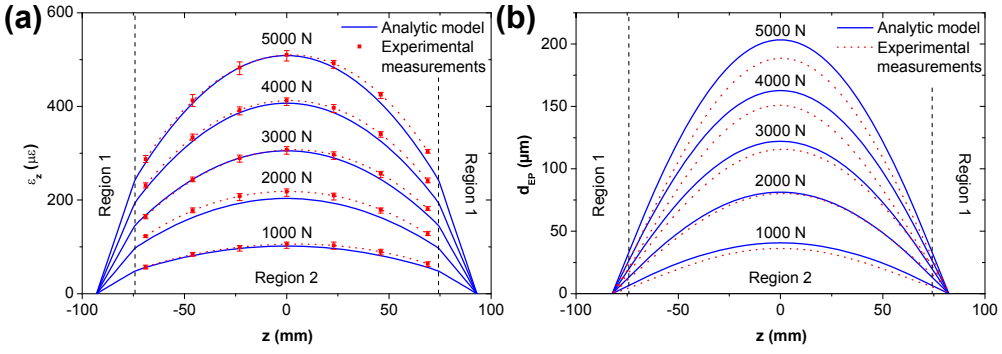

Fig. 13 – Comparison of a) ε_Z and b) d_{EP} between the results from the bending model and the experimental measurements.

Acknowledgments

It is a pleasure to acknowledge the "HYPLATE" FUI Project financed by the French Ministry of Economy and Finance, the ERDF and the Rhône-Alpes region. We specially thank all industrial partners of this project: AD Majoris (D. Beaudoux, B. Delamotte), Axane (E. Rossinot), IDI Composites International Europe (M.L. Guegan, J.P. Michaud) and Nief Plastic (D. Muller, O. Dassonville). Pierre Vacher is also greatly acknowledged for providing the 7D software. The "Assemblée des Pays de Savoie" is at last thanked for its financial contribution to the doctoral fellowship linked to this FUI project.

This work was performed in the Centre of Excellence of Multifunctional Architectured Materials "CEMAM".

REFERENCES

[1] Lee WK, Ho CH, Zee JWV, Murthy M. The effects of compression and gas diffusion layers on the performance of a PEM fuel cell. J Power Sources 1999;84(1):45–51.
[2] Wen CY, Lin YS, Lu CH. Experimental study of clamping effects on the performances of a single proton exchange membrane fuel cell and a 10-cell stack. J Power Sources 2009;192(2):475–85.
[3] Ge J, Higier A, Liu H. Effect of gas diffusion layer compression on PEM fuel cell performance. J Power Sources 2006;159(2):922–7.
[4] Chang HM, Lin CW, Chang MH, Shiu HR, Chang WC, Tsau FH. Optimization of polytetrafluoroethylene content in cathode gas diffusion layer by the evaluation of compression effect on the performance of a proton exchange membrane fuel cell. J Power Sources 2011;196(8):3773–80.
[5] Yim SD, Kim BJ, Sohn YJ, Yoon YG, Park GG, Lee WY, et al. The influence of stack clamping pressure on the performance of PEM fuel cell stack. Curr Appl Phys 2010;10(2, Suppl. 1):S59–61.
[6] Gatto I, Urbani F, Giacoppo G, Barbera O, Passalacqua E. Influence of the bolt torque on PEFC performance with different gasket materials. Int J Hydrogen Energy 2011;36(20):13043–50.
[7] Chang W, Hwang J, Weng F, Chan S. Effect of clamping pressure on the performance of a PEM fuel cell. J Power Sources 2007;166(1):149–54.
[8] Lin JH, Chen WH, Su YJ, Ko TH. Effect of gas diffusion layer compression on the performance in a proton exchange membrane fuel cell. Fuel 2008;87:2420–4.
[9] Escribano S, Blachot JF, Ethève J, Morin A, Mosdale R. Characterization of PEMFCs gas diffusion layers properties. J Power Sources 2006;156(1):8–13.
[10] Lee SJ, Hsu CD, Huang CH. Analyses of the fuel cell stack assembly pressure. J Power Sources 2005;145(2):353–61.
[11] Nitta I, Hottinen T, Himanen O, Mikkola M. Inhomogeneous compression of PEMFC gas diffusion layer: part I. Experimental. J Power Sources 2007;171:26–36.
[12] Hottinen T, Himanen O, Karvonen S, Nitta I. Inhomogeneous compression of PEMFC gas diffusion layer: part II. Modeling the effect. J Power Sources 2007;171:113–21.
[13] Wang X, Song Y, Zhang B. Experimental study on clamping pressure distribution in PEM fuel cells. J Power Sources 2008;179(1):305–9.
[14] Mikkola M, Tingelf T, Ihonen JK. Modelling compression pressure distribution in fuel cell stacks. J Power Sources 2009;193(1):269–75.
[15] Montanini R, Squadrito G, Giacoppo G. Experimental evaluation of the clamping pressure distribution in a PEM fuel cell using matrix-based piezoresistive thin-film sensors. In: Proc XIX IMEKO world congress; September 6–11 2009.
[16] Montanini R, Squadrito G, Giacoppo G. Measurement of the clamping pressure distribution in polymer electrolyte fuel cells using piezoresistive sensor arrays and digital image correlation techniques. J Power Sources 2011;196(20):8484–93.
[17] Carral C, Mélé P. Numerical analysis of stresses and strains in pemfc generated during cell assembly; 2012. Technoport RERC Research, Trondheim, Norway, April 16–18.
[18] Vacher P, Dumoulin S, Morestin F, Mguil-Touchal S. Bidimensional strain measurement using digital images. Proc Inst Mech Eng C J Mech Eng Sci 1999;213(8):811–7.
[19] The Technical Staff of Measurements Group, Inc.. Strain gage based transducers: their design and construction. Vishay Measurements Group; 1988.
[20] Ismail MS, Hassanpour A, Ingham DB, Ma L, Pourkashanian M. On the compressibility of gas diffusion layers in proton exchange membrane fuel cells. Fuel Cells 2012;12(3):391–7.
[21] Kleemann J, Finsterwalder F, Tillmetz W. Characterisation of mechanical behaviour and coupled electrical properties of polymer electrolyte membrane fuel cell gas diffusion layers. J Power Sources 2009;190(1):92–102.
[22] Bauchau O, Craig J. Euler-Bernoulli beam theory. In: Bauchau O, Craig J, editors. Structural analysis. Solid mechanics and its applications, vol. 163. Netherlands: Springer; 2009, ISBN 978-90-481-2515-9; 2009. pp. 173–221.